ECE Mechanism as a Tool for the Investigation of Unstable Metal Complexes. II. Current-Potential Characteristics for the Reversible Deposition of an Insoluble Species: Case of Electrochemical Reduction of *trans*-Dibromobis-(ethylenediamine)cobalt(III) Complexes

Akifumi YAMADA,* Tadatsugu YOSHIKUNI, Yoshikiyo KATO, and Nobuyuki TANAKA
Department of Chemistry, Faculty of Science, Tohoku University, Sendai 980
(Received September 6, 1979)

Theoretical relations were derived for the ECE mechanism involving the reversible deposition of an insoluble species at constant potential (potentiostatic method). Assuming that the activity of deposit becomes equal to unity immediately after the beginning of electrolysis, current-potential relations were obtained for the case in which the first electron transfer step is irreversible and the second one, reversible. The method was used to study the acid hydrolysis of bivalent cobalt complex in the reduction of *trans*-dibromobis(ethylenediamine)cobalt(III) complex. The measurement made at 5 °C in 0.1 M acetate buffer solutions (pH 4.8) gave 0.4 s^{-1} for the acid hydrolysis of *trans*-dibromobis(ethylenediamine)cobalt(II) which was produced by the reduction of cobalt(III) complex.

The ECE electrode reaction mechanism[1] has attracted attention in recent years in both theoretical and experimental fields. Theoretical studies have been carried out for electrochemical methods such as chronopotentiometry, potential step chronoamperometry, cyclic voltammetry, a.c. polarography, and d.c. polarography.[2]

Although experimental studies were carried out for the ECE electrode reaction of organic substances, only a few examples have been reported in inorganic electrochemistry.[3–11] In previous chronopotentiometric[8,9] and polarographic[7,10] studies, the rate constant of the complex-forming reaction for ethylenediaminetetraacetate and chromium(II) (electrochemically produced from chromium(III) complex) was successfully determined. The results have confirmed that the concept of ECE mechanism is useful for the study of an unstable intermediate electrochemically generated.

A test of the electrode reaction of cobalt(III) complexes revealed that the ECE mechanism involving reversible deposition of an insoluble species proceeds with complexes having ligands such as Cl^-, Br^-, and I^-. This was also pointed out by Vlček.[4] For example, the mechanism can be observed by the reduction of *trans*-dibromobis(ethylenediamine)cobalt(III) complex at the mercury electrode. When the cobalt(III) complex is reduced to cobalt(II), the cobalt(II) complex liberates bromide ions because of its lability. The electrochemically generated bromide ions are easily oxidized at the electrode to form insoluble mercury(I) bromide as long as the potential is positive. This series of electrode reaction takes place through the following electrode process:[12]

$$\textit{trans}\text{-}[CoBr_2(en)_2]^+ + e^- \longrightarrow \textit{trans}\text{-}[CoBr_2(en)_2], \quad (1)$$

$$\textit{trans}\text{-}[CoBr_2(en)_2] + 6H_2O \longrightarrow [Co(H_2O)_6]^{2+} + 2Br^- + 2en, \quad (2)$$

$$2Br^- + 2Hg \longrightarrow Hg_2Br_2 + 2e^-. \quad (3)$$

In this process, electrolytic deposition of an insoluble species is encountered. In order to include the reversible deposition of an insoluble species, an extension of the theory of the potentiostatic method for ECE mechanism seems necessary. This paper presents such an extension.

Experimental data were obtained for the potentiostatic reduction of *trans*-dibromobis(ethylenediamine)cobalt-(III) complex. The current-potential curves were compared with simulated ones. Calculation was made on the rate constant of the acid hydrolysis reaction of *trans*-dibromobis(ethylenediamine)cobalt(II) produced by the first electron transfer step.

Theoretical

ECE electrode reaction mechanism for many soluble species have been widely studied in the past,[1–11] but few quantitative analyses can be found for the ECE mechanism involving the reversible deposition of an insoluble species. This is understandable because of the inherent difficulty: the activity of the deposit cannot usually be known before the electrode becomes completely covered with at least a monolayer of deposit. In view of this we have considered a case in which it can be assumed that the activity of the deposit becomes equal to unity immediately after the beginning of electrolysis. For the sake of convenience, we describe the case which the first electron transfer step is irreversible and the second one reversible. This is the case for *trans*-$[CoBr_2(en)_2]^+$, and appears to be fairly general for ECE mechanism of halogenocobalt(III) complexes.[12]

The chronoamperometric technique applied to the analysis of the ECE mechanism has been described in detail by Alberts and Shain.[13] The boundary value problem for the electrode reaction

$$A + n_1e \xrightarrow{k_c} B \quad (4)$$

$$B \xrightarrow{l} C \quad (5)$$

$$C + n_2e \overset{E_0}{\rightleftharpoons} D \text{ (insoluble)} \quad (6)$$

is similar to that used by them, although specific boundary conditions are somewhat different. Here, A, B, C, and D represent the species, k_c is the heterogeneous rate constant, l the homogeneous rate constant, E_0 the standard potential of Reaction 6, and $n_j (j=1, 2)$ the number of electrons involved in the j-th electro-

chemical reaction: $n_j<0$ and $n_j>0$ correspond to reduction and oxidation, respectively. A, B, and C are soluble, and D is insoluble.

Assuming a linear diffusion, Fick's second law gives

$$\frac{\partial c_A}{\partial t} = D_A\left(\frac{\partial^2 c_A}{\partial x^2}\right), \tag{7}$$

$$\frac{\partial c_B}{\partial t} = D_B\left(\frac{\partial^2 c_B}{\partial x^2}\right) - lc_B, \tag{8}$$

$$\frac{\partial c_C}{\partial t} = D_C\left(\frac{\partial^2 c_C}{\partial x^2}\right) + lc_B, \tag{9}$$

where c and D are the concentration and diffusion coefficients, respectively, of a species indicated by subscripts, x is the distance from the electrode, and t the time.

The initial and boundary conditions are:

$$t = 0,\ x \geq 0\text{: } c_A = c^\circ,\ c_B = c_C = 0 \tag{10}$$

$$t \geq 0,\ x \to \infty\text{: } c_A = c^\circ,\ c_B, c_C \to 0 \tag{11}$$

$$t > 0,\ x = 0\text{:}$$

$$D_A\left(\frac{\partial c_A}{\partial x}\right)_{x=0} + D_B\left(\frac{\partial c_B}{\partial x}\right)_{x=0} = 0, \tag{12}$$

$$D_A\left(\frac{\partial c_A}{\partial x}\right)_{x=0} = k_c(c_A)_{x=0}, \tag{13}$$

$$(c_C)_{x=0} = \exp\left[\frac{n_2 F}{RT}(E-E_0)\right] = \theta, \tag{14}$$

where c° is the bulk concentration of A. Equation 14 represents a reversible deposition of the insoluble species D whose activity is assumed to be unity.

The equation for the total current is given by

$$I = Fq\left[n_1 D_A\left(\frac{\partial c_A}{\partial x}\right)_{x=0} + n_2 D_C\left(\frac{\partial c_C}{\partial x}\right)_{x=0}\right], \tag{15}$$

where F is the Faraday constant and q the electrode area. In this equation, anodic current is positive and cathodic current negative. This boundary value problem can be solved by means of the Laplace transform. The result is

$$\frac{I}{I_d} = \lambda\sqrt{\pi t}\exp(\lambda^2 t)\operatorname{erfc}(\lambda\sqrt{t}) - \frac{n_2}{n_1}\left(\frac{\theta}{c^\circ\sqrt{D_A/D_C}}\right) + \frac{n_2}{n_1}\left(\frac{D_C l}{D_C - D_B}\right)\lambda\sqrt{\pi t}\left[\exp(\lambda^2 t)\operatorname{erfc}(\lambda\sqrt{t}) * \exp\left(-\frac{D_C l t}{D_C - D_B}\right)\right] - \frac{n_2}{n_1}\sqrt{\frac{D_B}{D_C}}\left(\frac{D_C l}{D_C - D_B}\right)\lambda\sqrt{\pi t} \times\left[\frac{\exp(-lt)}{\sqrt{\pi t}} * \left\{\frac{1}{\sqrt{\pi t}} - \lambda\exp(\lambda^2 t)\operatorname{erfc}(\lambda\sqrt{t})\right\} * \exp\left(-\frac{D_C l t}{D_C - D_B}\right)\right], \tag{16}$$

with

$$\lambda = \frac{k_c^\circ}{\sqrt{D_A}}\exp\left[-\frac{\alpha n F}{RT}E\right] = \frac{k_c}{\sqrt{D_A}}, \tag{17}$$

$$I_d = \frac{n_1 F q c^\circ\sqrt{D_A}}{\sqrt{\pi t}}, \tag{18}$$

where k_c° is the heterogeneous rate constant at $E=0$ and α the transfer coefficient. The symbol $*$ represents the convolution.

It is evident from Eq. 16 that the current is stable when $D_C \geqq D_B$ but unstable or divergent when $D_C < D_B$. If $D_C < D_B$, peculiar phenomena might develop with time such as relaxational oscillations and jumps.

If Reaction 5 proceeds very rapidly and the condition $(D_C/D_B)\exp(lt) \gg 1$ is fulfilled, Eq. 16 is reduced to

$$\frac{I}{I_d} = \left(1+\frac{n_2}{n_1}\right)\lambda\sqrt{\pi t}\exp(\lambda^2 t)\operatorname{erfc}(\lambda\sqrt{t}) - \frac{n_2}{n_1}\left(\frac{\theta}{c^\circ\sqrt{D_A/D_C}}\right) - \frac{n_2}{n_1}\sqrt{\frac{D_B}{D_C}}\lambda\sqrt{\pi t}\int_0^t \frac{\exp[-l(t-u)]}{\sqrt{\pi(t-u)}} \times\left(\frac{1}{\sqrt{\pi u}} - \lambda\exp(\lambda^2 u)\operatorname{erfc}(\lambda\sqrt{u})\right)du. \tag{19}$$

If $lt \gg 1$, Eq. 19 can be further simplified to

$$\frac{I}{I_d} = \left(1+\frac{n_2}{n_1}\right)\lambda\sqrt{\pi t}\exp(\lambda^2 t)\operatorname{erfc}(\lambda\sqrt{t}) - \frac{n_2}{n_1}\left(\frac{\theta}{c^\circ\sqrt{D_A/D_C}}\right) - \frac{n_2}{n_1}\sqrt{\frac{D_B}{D_C}}\frac{\lambda}{\sqrt{l}} \times\left[\frac{1}{\sqrt{\pi t}} - \lambda\exp(\lambda^2 t)\operatorname{erfc}(\lambda\sqrt{t})\right]. \tag{20}$$

Equation 16 was solved numerically by the integral method of Gauss (Appendix). As expected, the computer results agree with the approximation given by Eq. 20 when the rate constant is large.

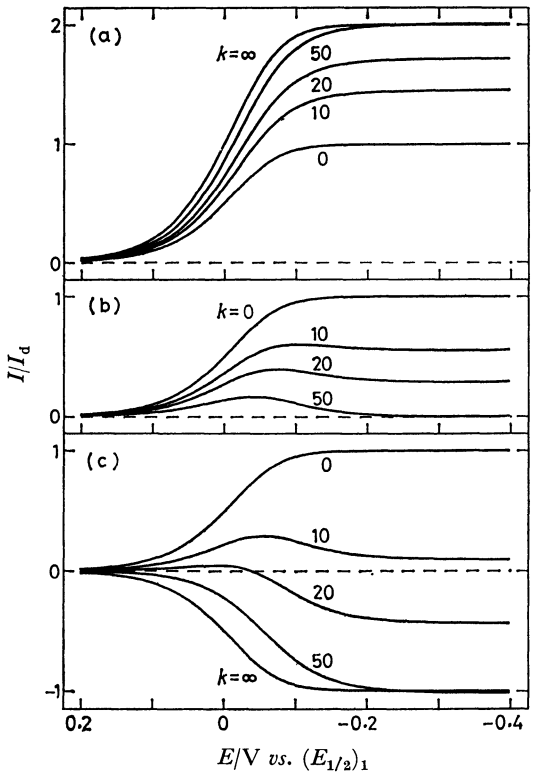

Fig. 1. Examples of predicted effects of homogeneous reaction rate on the current-potential curve for the consecutive ECE pathway (a) and the parallel ECE pathway (b, c).
Half-wave potential ($E_{1/2}$) and number of electrons (n) are: $(E_{1/2})_1=0$ V, $(E_{1/2})_2=+0.5$ V, $n_1=-1$, $n_2=-1$ for curve (a); $(E_{1/2})_1=0$ V, $(E_{1/2})_2=-0.5$ V, $n_1=-1$, $n_2=+1$ for curve (b); and $(E_{1/2})_1=0$ V, $(E_{1/2})_2=-0.5$ V, $n_1=-1$, $n_2=+2$ for curve (c). Other parameter values are: $T=25$ °C, $t=0.05$ s, $\alpha=0.5$, $D_A=B_B=5\times10^{-6}$ cm^2 s^{-1}, $D_C=10\times10^{-6}$ cm^2 s^{-1}. Homogeneous rate constants (in s^{-1}) are shown in figures.

According to Ruzic *et al.*[2] the ECE mechanism can be classified into a consecutive ECE pathway and a parallel one, the former dealing with the case where both heterogeneous steps are of the same type ($n_1n_2>0$), and the latter with heterogeneous electrode processes operating in the opposite direction ($n_1n_2<0$). Examples of the current-potential curve at various chemical reaction rates are shown in Fig. 1 for some interesting cases. Increase in current with increasing chemical reaction rate is seen for the consecutive ECE pathway (Fig. 1(a)), and decrease in current for the parallel ECE pathway (Fig. 1(b, c)). For a sufficiently fast chemical reaction the limiting current is diffusion-controlled for $n_1+n_2\neq 0$, but the net current is zero for $n_1+n_2=0$. This is a special case of parallel ECE pathway. Examples for $n_1+n_2=0$ are known for the electrode reaction of some chromium[6-10] and cobalt[3] complexes, though these are of soluble species.

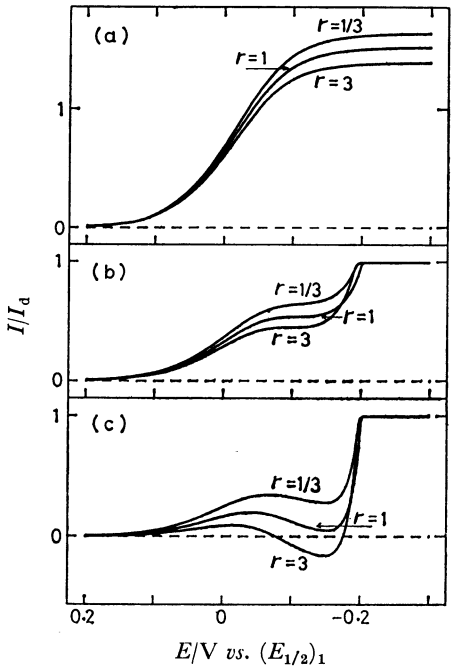

Fig. 2. Examples of predicted effects of the diffusion coefficient on current-potential curve for the consecutive ECE pathway (a) and the parallel ECE pathway (b, c). Ratios of diffusion coefficients of B and C (r) are shown in figures. Notation and parameter values are: $D_A=D_B=5\times10^{-6}$ cm^2 s^{-1}, $(E_{1/2})_1=0$ V, $l=15$ s^{-1}, $T=25$ °C, $t=0.05$ s, $\alpha=0.5$, $(E_{1/2})_2=+0.2$ V (a), -0.2 V (b, c). Number of electrons (n) are same as Fig. 1.

Figure 2 shows examples of the current-potential curve at different diffusion coefficients, calculated for the case of $D_B>D_C$, $D_B=D_C$, and $D_B<D_C$ when $D_A=D_B$. The effect of the diffusion coefficient on the current-potential curve dose not seem to be very small.

The current-potential curve should exhibit either one or two waves according to the difference in the half-wave potential of electrode reactions 1 and 3. This is shown clearly in Fig. 3, which depicts the current-potential curves with fast homogeneous chemical reactions.

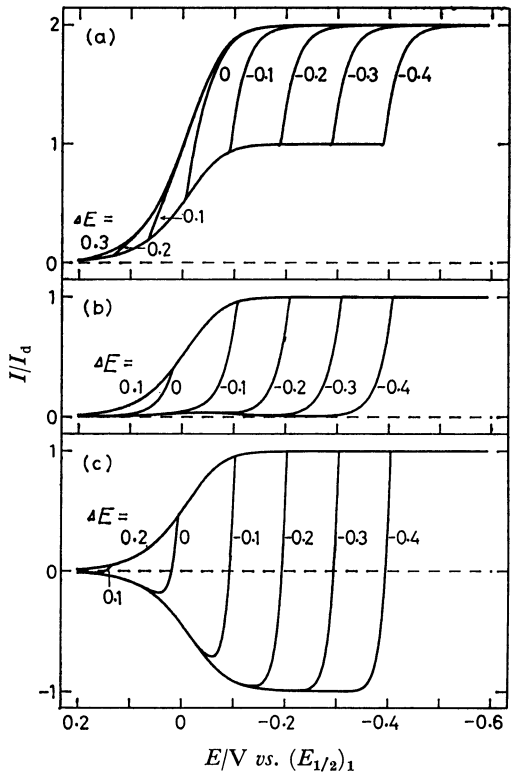

Fig. 3. Examples of predicted effects of the difference of half-wave potential corresponding to first and second electron-transfer steps on resolution of the current-potential curve for the consecutive ECE pathway (a) and the parallel ECE pathway (b, c). Potential differences ($\Delta E=(E_{1/2})_2-(E_{1/2})_1$) are shown in figures. Notation and parameter values are: $D_A=D_B=5\times10^{-6}$ cm^2 s^{-1}, $D_C=10\times10^{-6}$ cm^2 s^{-1}, $(E_{1/2})_1=0$ V, $l=100$ s^{-1}, $T=25$ °C, $t=0.05$ s, $\alpha=0.5$. Number of electrons (n) are same as Fig. 1.

When the two half-wave potentials are sufficiently separated with substance C which is more difficult to be reduced than A, the current-potential curve exhibits two waves (Fig. 3(a)). In this case, the current corresponding to the first wave represents the reduction of A only, depending on the kinetic parameters of the electrode reaction 1. The second wave is affected strongly by variation in the rate constant of chemical reaction 3. The current increases suddenly from the first wave, decreasing gradually after the diffusion current is reached.

When substance C is oxidized at a less positive potential than the reduction potential of substance A the cutoff of the first wave occurs: the decrease in current is pronounced with the increase in the rate of chemical reaction 2 (Fig. 3(b, c)). With $n_1+n_2=0$, the wave starts from the base line, increasing gradually. Theoretically, the slope of the current-potential curve should be infinite at the point where the current becomes diffusion-controlled. In the case $n_1+n_2>0$, the current starts from the anodic portion, increasing gradually. Then it decreases, crossing the zero current line. The final current is cathodic and controlled by Reaction 1. The shape of the current-potential curve is also angular at the beginning of the diffusion plateau.

Experimental

The current-potential curve were recorded with a Fuso Model 312 polarograph using a Watanabe Model WX441 x-y recorder. A three-electrode cell equipped with a saturated calomel reference electrode(SCE) and a platinum wire electrode(counter electrode) were employed. A junction of 0.1 M(1 M=1 mol dm^{-3}) $NaNO_3$ was used between the SCE and the solution in order to avoid chloride contamination. A dropping mercury electrode (flow rate 1.17 mg s^{-1}, drop time 3.97 s in 0.1 M acetate buffer solutions) was used as a working electrode.

The complex used was prepared according to the procedure of Werner *et al.*[14] and identified by elemental analysis. A small amount of gelatin was added as a maximum suppressor.

Results and Discussion

Current-Potential Behavior. Figure 4 shows the current-potential curves of 0.5 mM *trans*-$[CoBr_2(en)_2]NO_3$ and 0.5 mM KBr obtained in 0.1 M acetate buffer solution at 25 °C. As expected from the electrode reaction of other cobalt(III) complexes,[15] *trans*-$[CoBr_2(en)_2]^+$ gave two polarographic waves, the first corresponding to the reduction of Co(III) to Co(II) and the second to the reduction of Co(II) to Co(0).

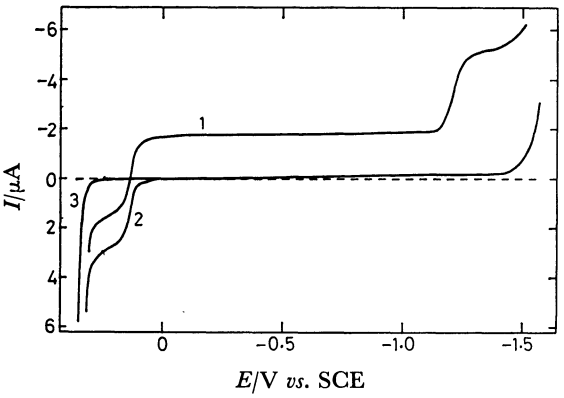

Fig. 4. Current-potential curves of (1) 0.5 mM *trans*-$[CoBr_2(en)_2]NO_3$ and (2) 0.5 mM KBr obtained in (3) 0.1 mM acetate buffer solutions containing 0.005% gelatin at 25 °C.

The first wave appears partly above and partly below the zero current line on the polarogram in Fig. 4. The cathodic limiting current of the first wave was diffusion-controlled and proportional to the concentration of the complex. The anodic limiting current of the first wave was also diffusion-controlled. The diffusion coefficients of the complex and Br^- ions were determined by means of the method reported.[16] The values are: 8.32×10^{-6} $cm^2\,s^{-1}$ for *trans*-$[CoBr_2(en)_2]^+$ and 25.1×10^{-6} $cm^2\,s^{-1}$ for Br^- at 25 °C and ionic strength 0.1.

The magnitude of the anodic current of the first wave was found to be identical with that of the cathodic one which corresponds to the reduction of Co(III) to Co(II). The first wave was very similar in shape to the dissolution wave of the mercury in the presence of Br^- ions (Fig. 4). This suggests that the mass transport toward the electrode is controlled not by the diffusion of Br^- ions but by that of *trans*-$[CoBr_2(en)_2]^+$. The shape of the first wave also indicates that the current-potential curve is characterized mainly by the anodic depolarization wave of Br^- ions. Thus, the overall electrode reaction in acid media might be expected to follows a mechanism given by Eqs. 1—3.

If we classify the ECE mechanism into the two types, consecutive and parallel ECE pathways,[2] the electrode reaction of *trans*-$[CoBr_2(en)_2]^+$ belongs to the parallel case. When the tervalent cobalt complex is reduced to the bivalent one, the substitution-labile bivalent complex liberates 2 mol of Br^- ions and dissolution wave of mercury by Br^- ions appears. This gives rise to the net current anodic. When the electrode potential becomes negative, dissolution ceases and a wave appears with a half-wave potential nearly equal to that of the anodic depolarization wave of Br^- ions.

The foregoing situation corresponds to the curve at $\Delta E=-0.3$ or -0.4 V (Fig. 3(c)) which depicts a global shape of the simulated parallel ECE pathway for $n_1=+2$. Strictly speaking, n_2 should be replaced by $2n_2$ for the electrode reaction of *trans*-$[CoBr_2(en)_2]^+$. Details are given below. In order to confirm the theory, a current-potential curve was simulated and the result compared with the measured one.

Simulation of Current-Potential Curve. Current-potential curves at more positive potential were obscured by the free dissolution wave of mercury.[17] However, both anodic and cathodic waves of *trans*-$[CoBr_2(en)_2]^+$ were resolved, each showing a limiting current plateau (Fig. 4). Thus, the half-wave potential of Reaction 1 would lie at least 0.3 V more positive than that of Reactions 3 as expected from Fig. 3(c). The current under these conditions does not depend on the heterogeneous rate constant of Reaction 1, but on the homogeneous rate constant of Reaction 2 as well as on the characteristics of electrode reaction 3.

The implicit solution of Eq. 16 is given in the Appendix. The current is given by Eq. A-2, where λ is made infinite and n_2 is replaced by $2n_2$ since 2 mol of Br^- ions are liberated from 1 mol of complex (Reaction 2). Thus, we have

$$\left(\frac{I}{I_d}\right)_{\lambda\to\infty} = 1-\frac{2n_2}{n_1}\left(\frac{\theta}{\sqrt{D_A/D_C}c^\circ}\right)+\frac{2n_2}{n_1}\phi(a\sqrt{t}) - \frac{2n_2}{n_1}\sqrt{\frac{D_C}{D_B}}\exp(-lt)\phi\left(\sqrt{\frac{D_B}{D_C}}a\sqrt{t}\right), \quad (21)$$

with

$$\phi(x) = 2x\exp(-x^2)\int_0^x \exp(u^2)\mathrm{d}u, \quad (22)$$

where $a=\sqrt{D_C l/(D_C-D_B)}$.

For the sake of approximation, plane electrodes were assumed for derivation. This is because the corresponding derivation for an expanding plane electrode would be far more difficult and the activity of deposit during the course of expansion is not be known until the electrode is completely covered with deposit. Our data represent a preliminary study to demonstrate some phenomena predicted theoretically.

In the range of anodic current plateau, θ in Eq. 21 becomes zero. It follows that

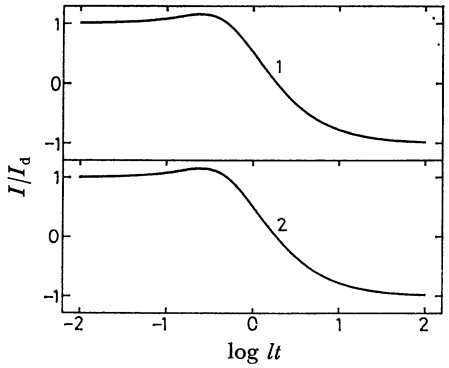

Fig. 5. Working curves for calculation of homogeneous rate constant. Diffusion coefficients are: (1) $D_A=D_B=8.32\times10^{-6}$ cm^2 s^{-1}, $D_C=25.1\times10^{-6}$ cm^2 s^{-1} and (2) $D_A=D_B=4.67\times10^{-6}$ cm^2 s^{-1}, $D_C=13.7\times10^{-6}$ cm^2 s^{-1}.

$$\frac{I}{I_d}=1+\frac{2n_2}{n_1}\left[\phi\left(\sqrt{\frac{D_C lt}{D_C-D_B}}\right)-\sqrt{\frac{D_C}{D_B}}\exp(-lt)\phi\left(\sqrt{\frac{D_B lt}{D_C-D_B}}\right)\right]. \quad (23)$$

In order to evaluate the rate constant, the value of I/I_d was calculated against lt and is plotted in Fig. 5 for two sets of diffusion coefficients. In this calculation, curve 1 corresponds to the case at 25 °C ($D_A=D_B=8.32\times10^{-6}$ cm^2 s^{-1}, $D_C=25.1\times10^{-6}$ cm^2 s^{-1}) and curve 2, to the case of 5 °C ($D_A=D_B=4.67\times10^{-6}$ cm^2 s^{-1}, $D_C=13.7\times10^{-6}$ cm^2 s^{-1}).

The value of I/I_d at +0.25 V *vs.* SCE was found to be 1 at 25 °C. This indicates that the acid hydrolysis reaction 2 proceeds very rapidly. The rate constant was obtained by varying temperature. The measurement made at 5 °C gave $l=0.4$ s^{-1} for the acid hydrolysis rate constant. The value was determined from the working curve 2 in Fig. 5. Reliability of the rate of Reaction 2 was tested by the following simulation of current-potential curves.

The preceding preliminary estimation indicates $(D_C/D_B)\exp(lt)\gg1$. Thus, Eq. 21 can be simplified to

$$\frac{I}{I_d}=1+\frac{2n_2}{n_1}\left(1-\frac{\theta}{c^\circ\sqrt{D_A/D_C}}\right)-\frac{2n_2}{n_1}\sqrt{\frac{D_B}{D_C}}\exp(-lt). \quad (24)$$

If $\theta=0$ and $D_B=D_C$, the relation agrees with the equation of Alberts and Shain.[13] In Eq. 24 the second term represents the depolarization term of Br$^-$ ions at mercury electrode, which can be calculated from the dissolution wave of mercury in the presence of Br$^-$ ions only. The anodic dissolution wave with Br$^-$ ions is given by[18]

$$I=(I_d)_C\left(1-\frac{\theta}{c^*}\right), \quad (25)$$

where $(I_d)_C=n_2Fqc^*\sqrt{D_C}/\sqrt{\pi t}$. Thus, $1-\theta/c^\circ\sqrt{D_A/D_C}$, which is required in the calculation of Eq. 24, can be obtained experimentally from the current-potential curve at $c^*=c^\circ\sqrt{D_A/D_C}$.

The simulated current-potential curves for the reduction of *trans*-$[CoBr_2(en)_2]^+$ at 25 °C and 5 °C are shown in Fig. 6 together with the experimental data. Curve 1 for $l>3$ s^{-1} and curve 2 for $l=0.4$ s^{-1}. In this

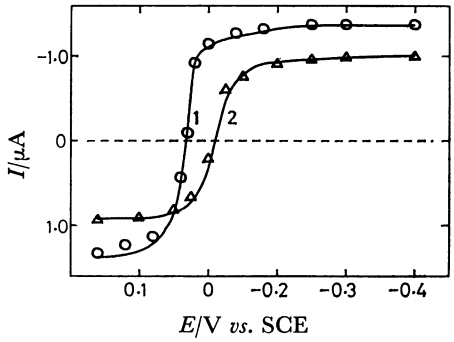

Fig. 6. Comparison of observed and simulated current-potential curves for the reduction of *trans*-$[CoBr_2(en)_2]NO_3$ at (1) 25 °C and (2) 5 °C. Circles and triangles, experimental; solid lines, theoretical.

calculation, when the current-potential curve of Br$^-$ ions was used for $c^*=c^\circ\sqrt{D_A/D_C}$, the zero-cross potential was *ca.* 25 mV more positive than the observed one. Good agreement was obtained by taking a value of $c^*=0.7$ mM for curve 1 and $c^*=0.6$ mM for curve 2. These values were used to construct the current-potential curves shown in Fig. 6. The discrepancy between theory and experiment is most likely due to the change in the activity of insoluble film.

The calculation given in Fig. 6 basically conforms to the concept of parallel ECE pathway. The current-potential behavior of *trans*-$[CoBr_2(en)_2]^+$ is thus in line with the overall mechanism given by Reactions 1—3 in which the parallel ECE pathway occurs.

Appendix

The boundary value problem stated by Eqs. 7—15 was solved by a straight-forward application of the laplace transformation. The following equation was obtained for the current:

$$I(s)=n_1Fc^\circ\sqrt{D_A\lambda}\frac{1}{\sqrt{s}(\sqrt{s}+\lambda)}+n_2F\sqrt{D_A}\left(\frac{D_C l}{D_C-D_B}\right)c^\circ\lambda\times\frac{1}{\sqrt{s}(\sqrt{s+\lambda})\left(s+\frac{D_C}{D_C-D_B}l\right)}-n_2F\sqrt{D_C}\theta\frac{1}{\sqrt{s}}-n_2F\sqrt{D_A}\sqrt{\frac{D_B}{D_C}}\left(\frac{D_C l}{D_C-D_B}\right)c^\circ\lambda\times\frac{1}{\sqrt{s+1}(\sqrt{s}+\lambda)\left(s+\frac{D_C l}{D_C-D_B}\right)}. \quad (A\text{-}1)$$

The inverse transform of this expression can be found by using the convolution theorem[19] which is

$$L^{-1}[f_1(s)\cdot f_2(s)]=\int_0^t F_1(u)F_2(t-u)\mathrm{d}u=F_1(t)*F_2(t)$$

with $L[F_1(t)]=f_1(s)$ and $L[F_2(t)]=f_2(s)$.

Equation 16 is obtained from the table of Laplace transform pairs.[19]

For the numerical calculation, Eq. 16 can be rewritten as

$$\frac{I}{I_d}=\lambda\sqrt{\pi t}\exp(\lambda^2 t)\operatorname{erfc}(\lambda\sqrt{t})-\frac{n_2}{n_1}\left(\frac{\theta}{c^\circ\sqrt{D_A/D_C}}\right)+\frac{n_2}{n_1}(\pm a^2)\lambda\sqrt{\pi t}\exp(\mp a^2 t)$$

$$\times\int_0^t \exp\left[(\lambda^2\pm a^2)u\right]\operatorname{erfc}(\lambda\sqrt{u})\,du$$

$$-\frac{n_2}{n_1}\sqrt{\frac{D_B}{D_C}}\lambda\sqrt{\pi t}\left(\frac{\pm a^2}{\lambda^2\pm a^2}\right)\int_0^t G(u)H(t-u)\,du \qquad \text{(A-2)}$$

with

$$G(u) = \exp(\mp a^2u)\left[\lambda\pm a\frac{2}{\sqrt{\pi}}\int_0^{a\sqrt{u}}\exp(\pm r^2)\,dr\right] - \lambda\exp(\lambda^2u)\operatorname{erfc}(\lambda\sqrt{u}) \qquad \text{(A-3)}$$

$$H(u) = \frac{\exp(-lu)}{\sqrt{\pi u}} \qquad \text{(A-4)}$$

where $a=\sqrt{D_Cl/(D_C-D_B)}$. The upper sign holds if $D_C>D_B$, the lower if $D_C<D_B$. Equation A-2 was computed numerically by the intergral method of Gauss.[20] The change of variable, $x=\sqrt{t-u}$, was employed in order to remove the singularity at $u=t$.

The function $\sqrt{\pi}x\exp(x^2)\operatorname{erfc}(x)$ in Eq. A-2 was calculated by a method described previously.[21]

The research was carried out by a Grant-in-Aid from the Ministry of Education. A part of the work was supported by Scientific Research Grant No. 364205.

References

1) A. C. Testa and W. H. Reinmuth, *Anal. Chem.*, **33**, 1320 (1961).
2) I. Ruzic, H. R. Sobel, and D. E. Smith, *J. Electroanal. Chem.*, **65**, 21 (1975) and the references cited therein.
3) H. A. Laitinen and P. Kivalo, *J. Am. Chem. Soc.*, **75**, 2198 (1953).
4) A. A. Vlček, "Polarographic Behavior of Coordination Compounds," in "Progress in Inorganic Chemistry," ed by F. A. Cotton, Interscience Publishers, New York (1963), Vol. 5, pp. 211—384.
5) K. Ebata, *Sci. Repts. Tohoku Univ., Ser. I*, **47**., 191 (1964).
6) N. Tanaka and K. Ebata, *J. Elecrtoanal. Chem.*, **8**, 120 (1964).
7) K. Ogino and N. Tanaka, *Bull. Chem. Soc. Jpn.*, **39**, 2672 (1966).
8) N. Tanaka and A. Yamada, International Congress of Polarography, Kyoto, September 1966, Abstr. p. 124.
9) N. Tanaka and A. Yamada, *Rev. Polarog. (Kyoto)*, **14**, 234 (1967).
10) E. Fisherova, O. Drăcka, and M. Meloun, *Collect. Czech. Chem. Commun.*, **33**, 473 (1968).
11) S. W. Feldberg and L. Jeftic, *J. Phys. Chem.*, **76**, 2439 (1972).
12) N. Tanaka, Y. Yoshikuni, Y. Kato, and A. Yamada, *J. Electroanal. Chem.*, **107**, 95 (1980).
13) G. S. Alberts and I. Shain, *Anal. Chem.*, **35**, 1859 (1963).
14) A. Werner, L. Gerb, S. Lorie, and J. Rapiport, *Ann.*, **386**, 111 (1912).
15) N. Maki and N. Tanaka, "Encyclopedia of Electrochemistry of the Elements," ed by A. J. Bard, Marcel Dekker Inc., New York (1975), Vol. 3, pp. 43—210.
16) A. Yamada, Y. Kato, T. Yoshikuni, Y. Tanaka, and N. Tanaka, *Anal. Chim. Acta*, **112**, 55 (1979).
17) I. M. Kolthoff and J. J. Lingane, "Polarography," Interscience Publishers, New York (1964), Vol. 2, pp. 577—581.
18) P. Delahay, "New Instrumental Methods in Electrochemistry," Interscience Publishers, New York (1954), p. 57.
19) R. V. Churchill, "Operational Mathematics," 2nd ed, McGraw-Hill Book Company, Inc., New York (1958).
20) H. Margenau and G. M. Murphy, "The Mathematics of Physics and Chemistry," D. Van Nostrand Company, Inc., Princeton, New Jersey (1943).
21) A. Yamada and N. Tanaka, *Anal. Chem.*, **45**, 167 (1973).